JOURNAL OF PROPULSION AND POWER
Vol. 23, No. 4, July–August 2007

Characterization of Nanometer- to Micron-Sized Aluminum Powders: Size Distribution from Thermogravimetric Analysis

Curtis E. Johnson,* Stephen Fallis,* Andrew P. Chafin,* Thomas J. Groshens,* and Kelvin T. Higa*
U.S. Naval Air Systems Command, China Lake, California 93555
and
Ismail M. K. Ismail† and Tom W. Hawkins‡
U.S. Air Force Research Laboratory, Edwards Air Force Base, California 93524

DOI: 10.2514/1.25517

Thermogravimetric analysis was used to study the reactivity of aluminum powders in air, oxygen, and nitrogen. In addition, the data were used to characterize active Al content, Al oxide content, volatile impurity content, particle size, and particle size distribution. Weight gains from complete oxidation of the Al were used to calculate average particle sizes in the range of 30 to 500 nm. These particle sizes correlated well with particle sizes derived from surface area measurement. Particle size was also examined by scanning electron microscopy, and compared with crystallite size determined by x-ray diffraction. Particle size distributions were derived from thermogravimetric analysis data based on a model of uniform oxidation of Al from the exterior to the interior of the particle. The method is well suited for analyzing samples with broad particle size distributions, and in particular, for monitoring the presence of 500–5000 nm particles within nominally nanosized samples. Quantitative information was not obtained for particles around 100 nm or smaller, due to large variations in oxidation behavior below 700°C. Nitridation of Al powders was studied for extended times at 600°C. Surprisingly, 2 μm powder was nearly completely nitrided in 1 h, indicating that the nitride product has little inhibiting effect on the reaction.

Introduction

ALUMINUM powders are used in a broad range of applications including rocket propellants, paints, and powder metallurgy processes for aircraft and automobile parts [1,2]. Because the reactivity of Al increases as the particle size decreases, small particles are desirable for Al used in propellants, explosives, and powder metallurgy processes.

Aluminum powders are produced on a large scale in the nominal size range of 3–200 μm. Over the last decade submicron Al powders have become commercially available in significant quantities and with selected sizes in the range of 20 to 500 nm. As these powders are beginning to find their way into applications, there is a need to develop specifications and standard characterization procedures [3] to ensure consistency of the material and its behavior. Key attributes of Al powders include particle size, size distribution, particle morphology, agglomeration, and chemical composition (especially metallic Al and Al oxide content). Commercial powders are typically supplied with a particle size derived from surface area analysis. Many users of nanosized Al powders conduct additional analysis to gain information about chemical composition, particle morphology, and particle size distribution.

Variations in particle size distribution may significantly affect reactivity [4]; however, the particle size distribution of nanopowders has been difficult to quantify by conventional particle size measurements. Nanopowders tend to form aggregates that only partially disperse for particle size analysis by light scattering methods [5]. Many aluminum nanopowders exhibit broad size distributions, with the size distribution dependent in part on the method of synthesis [6]. Some powders appear to have a lognormal size distribution, where the logarithm of the particle diameter has a Gaussian distribution [7], whereas a bimodal distribution was reported for an Al powder prepared by an electroexplosion process [8]. Useful particle size distribution information can be obtained by scanning electron microscopy (SEM), transmission electron microscopy (TEM) [9–14], small angle neutron scattering (SANS), or small angle x-ray scattering analysis (SAXS) [13,15–18]. Quantitative analysis of particle size distribution by SEM or TEM is usually problematic in dispersing and resolving individual nanoparticles, and achieving analysis of a representative portion of the material. Representative sampling can be particularly difficult for broad size distributions or for samples with occasional large particles. Large particles do not transmit the electron beam, limiting TEM analysis. Sampling is not a problem for SAXS or SANS, but the techniques applied to date to aluminum nanopowders are relatively insensitive to micron-sized particles, and considerable data interpretation is involved in the analysis. The size distributions for some aerosolized aluminum nanopowders were recently determined using a differential mobility analyzer with a condensation particle counter [19,20].

Thermogravimetric analysis (TGA) of the oxidation of submicron Al powders is a valuable characterization technique as it provides information about both reactivity and composition [9,21–23]. Data from TGA experiments has been used to determine activation energies [9,22,24–26], active aluminum content [21,27], initial oxide layer thickness [28–30], and particle size [21]. In the present paper, we explore the utility of thermogravimetric analysis in characterizing submicron Al powders and their reactivity to air, nitrogen, and oxygen. Curve-fitting procedures were developed to calculate particle size distributions from the TGA data [31].

Experimental Methods

The "ALEX" aluminum powder was obtained from the Argonide Corporation and was prepared by an electroexplosion process using

Received 2 June 2006; revision received 7 February 2007; accepted for publication 30 March 2007.

*Research Chemist, Chemistry and Materials Division, Code 498200D, 1900 North Knox Road, Stop 6303.

†Senior Engineer Scientist, Propulsion Directorate, Space and Missile Division, Propellant Branch; currently Senior Engineer Scientist, ERC, Inc., Huntsville, AL 35816.

‡Senior Research Scientist, Propulsion Directorate, Space and Missile Division, Propellant Branch.

Al wire. Vapor condensation processes were used in the preparation of Al powders provided by Los Alamos National Laboratory ("LANL" powders), Naval Surface Warfare Center, Indian Head Division ("IH-1"), and Technanogy ("Tech 24," "Tech 52," "Tech 73," "Tech 192," and "Tech 455"). The "H-2," "H-3," and "H-5" powders were obtained from Valimet and were prepared by a gas atomization process. The remaining Al powders with CL designations were prepared by a solution process involving the catalyzed decomposition of trialkyl amine adducts of alane (AlH_3) at 40–110°C [21,32,33]. Titanium isopropoxide was used as the catalyst, and most of the titanium was reduced and incorporated in the Al. The molar ratio of catalyst to Al was: 0.1% for CL-01 and 40; 0.15% for CL-B, J, and K; 0.2% for CL-57; 0.5% for CL-06, 35, and 48; 2% for CL-10, 11, and 96; 3% for CL-41; and 10% for CL-49. After passivation of the Al by controlled exposure to air, samples were dried as follows to remove organic contaminants: CL-57 was dried in air at room temperature, samples CL-B, J, and K were dried under vacuum at room temperature, and the remaining CL samples were dried under vacuum for about 30 min at 210°C, then cooled to room temperature before exposing to air.

The active (or metallic) Al content in powders was determined by quantitatively measuring either the gas evolved upon base hydrolysis [34], or the weight gain upon thermal oxidation to aluminum oxide. For the hydrolysis method, ~0.2-g samples were completely hydrolyzed in 1 M NaOH or KOH aqueous solution. The weight percent of active Al in the sample was calculated based on the stoichiometry in Eq. (1):

$$\mathrm{Al} + \mathrm{OH}^- + 3\mathrm{H_2O} = \mathrm{Al(OH)_4^-} + \tfrac{3}{2}\mathrm{H_2} \qquad (1)$$

Reported results are the average of three runs. Estimated accuracy is ±2%.

Scanning electron microscopy was conducted on an Electroscan Environmental Model E-3 in the presence of water vapor at about 600 Pa, and an Amray Model 1400 instrument. X-ray powder diffraction patterns were obtained from petrolatum (Vaseline) mounted samples on glass slides using a Scintag PAD V diffractometer with Cu K_α radiation. Average crystallite sizes were calculated from x-ray linewidths using the Scherrer equation [35], and software provided with the instrument (DMSNT version 1.37 software with Crystallite Size software package version 1.01). Linewidths were corrected for instrument parameters determined from a reference scan of a NIST SRM alumina plate. Reported values are the average of four sizes calculated from peaks at $2\theta = 38, 44, 65,$ and 78°.

Thermogravimetric analysis (TGA) in flowing air and oxygen (99.995% purity) was conducted on a TA Instruments 2950 thermogravimetric analyzer with a DuPont 2100 thermal analyst controller. The highest temperature used in these experiments was 950°C due to the 1000°C limit of the instrument. Sample weights ranged from 1–5 mg and weight data were corrected for the instrumental baseline response, based on blank (empty Al oxide pan) experiments conducted periodically. The standard TGA experiment was to heat the sample to 850°C and hold at that temperature for 4 h. A steady ramp of 20°C/ min was used for samples CL-B, CL-J, CL-K, LANL-1, and LANL RF19. For the remaining samples, quantitative analysis was generally conducted with the ramp rate slowed to 3°C/ min in the temperature range of 350–600°C. The lower heating rate was chosen to prevent ignition of samples, which sometimes occurred at 500–600°C. When samples were analyzed by both heating programs, the TGA curves were very similar, but a local minimum in oxidation rate occurred at about 690°C for the constant 20°C/ min ramp, compared with 590–600°C for the 3°C/ min ramp.

A second TGA apparatus was used for thermogravimetric analysis under nitrogen, where the isothermal increase in sample weight was monitored as a function of time at ambient pressure. This apparatus, shown schematically in Fig. 1, was better suited to providing an ultrahigh purity nitrogen environment, which facilitated the nitridation reaction of aluminum. The TGA apparatus contained four main components: a CAHN-2000 electrobalance with a cylindrical quartz sample container (bucket) suspended on the balance beam, a vertical furnace surrounding the reactor, a roughing pump attached to an oil diffusion pump with a cryogenic stack, and a set of three MKS® transducer heads (133, 1330, and 133,000 Pa). To start a run, a small weight of the powder, normally 12–15 mg, was placed in the quartz bucket, suspended on the balance beam, and evacuated to 10^{-4} Pa for 2 h. The sample was brought to ambient pressure using ultrahigh pure nitrogen (>99.999% purity) at atmospheric pressure for 30 min. The concentration of impurities in the nitrogen stream, as supplied by the manufacturer, was as follows: 0.382 part per million (ppm) moisture, 0.5 ppm oxygen, 0.1 ppm total hydrocarbons, <1 ppm CO_2 and <1 ppm CO. Samples were heated at 35°C/ min to an isothermal temperature of 600°C under a nitrogen flow rate of 50 cm^3/ min. The increase in sample weight, attributed to the reaction $2Al + N_2 \rightarrow 2AlN$, was followed with time. The increase in weight was monitored as a function of time until the

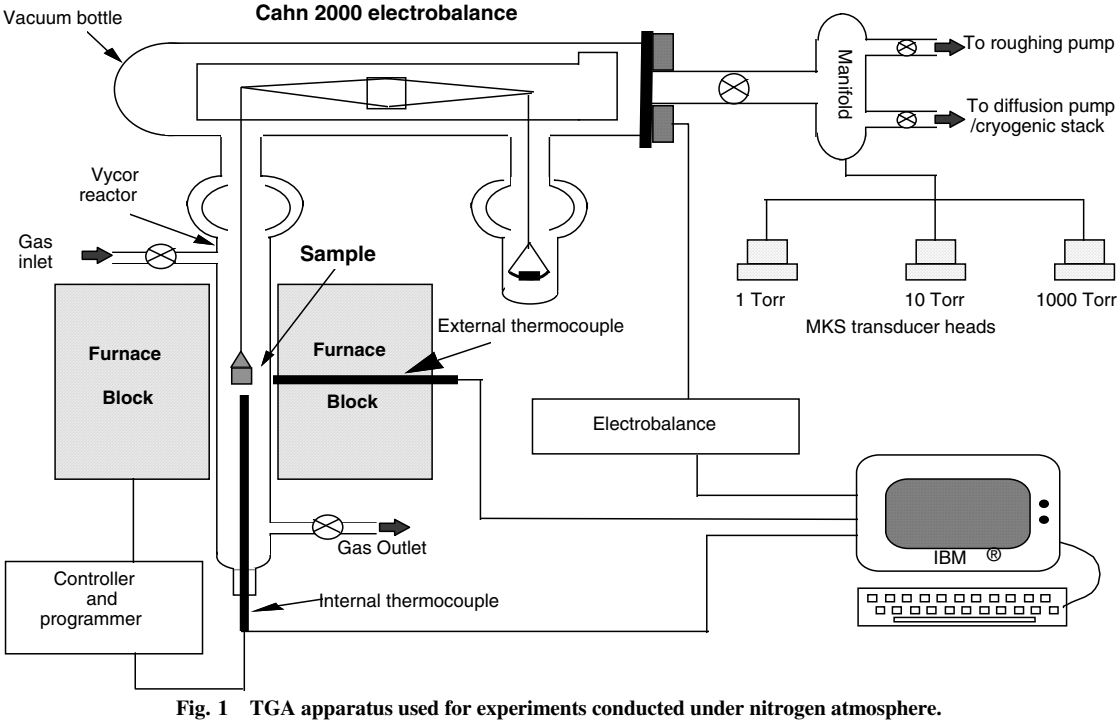

Fig. 1 TGA apparatus used for experiments conducted under nitrogen atmosphere.

weight increase became insignificant or when sample weight remained practically constant.

The surface area of Al powders was determined by conventional volumetric gas adsorption technique using either a Micromeritics Digisorb 2600 or a Quantachrome Autosorb-1C surface area analyzer. Before each measurement, the powder was heated under vacuum, in most cases at 250°C for 24 h. This treatment removed the foreign species adsorbed at the surface such as CO_2, H_2O, oils, and grease. After the pretreatment, the evacuated samples were immersed in a liquid nitrogen bath and the adsorption isotherms of nitrogen at −196°C were obtained. At least two runs were conducted for each sample, and the results averaged. The isotherms on all powders were of type II, indicating that the Al powders examined here are typical nonporous materials [36]. To calculate the surface area from the isotherms, the Brunauer, Emmett and Teller (BET) equation was used [37].

Experimental Curve-Fitting Procedures

The experimental TGA curve can be thought of as a weighted sum of TGA curves of samples with narrower size distributions. Therefore, the particle size distribution of the sample can be found by fitting the experimental TGA curve with a weighted sum of TGA curves from samples with narrower size distributions. These curves with narrower size distributions are the "basis curves." Each sample for the basis curves would ideally be monomodal with a very narrow distribution. Combined, the sizes of the samples for the basis curves must span the expected distribution of any experimental samples. In this paper we examine two types of basis curves, empirical basis curves and those derived from a "master curve."

Empirical Basis Curves

The calculation of a curve from a set of basis curves is straightforward. The weight fraction of each size is used as a weighting factor for the basis curve. The weighted basis curves are added together to form the calculated curve. The weightings are then optimized to give the best fit to the experimental TGA curve. The empirical basis curves were taken from a set of experimental TGA curves on samples that appeared to have relatively narrow size distributions, based on both SEM and TGA characterization (see Results and Discussion section). The weight data were normalized by dividing the observed weight by the minimum weight reached after volatile contaminants were lost (typically occurred at about 350°C). The data were then smoothed and interpolated to give a set of curves having the same time scale and intervals. These empirical basis curves are shown in Fig. 2, with nominal sizes given for each sample.

The fitting procedure starts by normalizing, smoothing and interpolating the experimental curve. A mean particle size is estimated by the procedure above and is used as the starting point by interpolating between the two closest basis curves. During the constrained optimization the weight factor for each pair of basis curves is varied (one up and one down to keep the total weight fraction at 1.0) and a new curve is calculated. The deviation from the experimental curve is squared and compared with the previous point. If lower, the new point is kept, or else it is discarded. In this way all possible combinations are examined. After a complete round without any points kept, the step size is reduced and the procedure started again. The procedure is stopped when the step size falls below 0.0001.

For this procedure to converge to a global minimum the basis curves must be as orthogonal as possible. In the present situation, the basis curves with small average size diverge from each other at the beginning of the curve, whereas those with large average size diverge at the end of the curve.

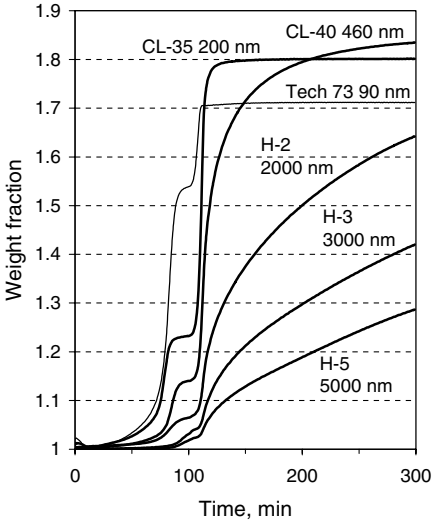

Fig. 2 TGA curves for six aluminum samples used as a basis set for empirical curve fitting. Heating program: 20°C/min to 350°C, 3°C/min to 600°C, 20°C/min to 850°C, hold at 850°C for 4 h.

Master Curve

Ideally, the basis curves used for curve fitting would each represent a single particle size. This would be possible if a mathematical model of the oxidation process was used. The model used in this work assumes that the samples consist of spherical particles that are uniformly oxidized from the outside in, independent of particle size. This model was used to convert experimental weight vs time TGA curves into curves of thickness of aluminum oxidized vs time. According to the model, the thickness of aluminum oxidized curves for different particle sizes would all overlap if each sample was monosized. Thus, the thickness of aluminum oxidized curves for 14 samples were averaged to give a single "master curve." From this master curve, theoretical basis curves for single particle sizes were calculated and used in the optimization procedure.

The 14 samples used to generate the master curve were chosen to have relatively narrow size distributions and cover a broad range of sizes. The six samples chosen in the previous section on empirical basis curves (see Fig. 2) were included in the master curve sample set. The other eight samples with their nominal particle size are: CL-01 (256 nm), CL-48 (138 nm), CL-11 (73 nm), Tech 52 (66 nm), CL-41 (63 nm), LANL RF-A (49 nm), Tech 24 (28 nm), and IH-1 (15 nm). Each experimental TGA curve was corrected by subtracting a background curve that was obtained by subjecting an empty sample pan to the same temperature program in the TGA. The curves were then normalized to have a minimum weight fraction of 1.0 by dividing the observed weight by the minimum weight. Smoothing and interpolation gave a set of curves having the same time scale and intervals. The weight fraction data were then converted to thickness of aluminum oxidized using the analysis described in detail in the following paragraphs. Figure 3 shows plots of thickness of aluminum oxidized vs time for the 14 samples.

After the loss of volatile contaminants in the TGA experiment, the particles were considered to consist of an Al core with density 2.702 g/cm^3 (d_{Al}), and an Al oxide passivation layer with a thickness of 2.5 nm ($t_{Al_2O_3}$) and density 3.965 g/cm^3 ($d_{Al_2O_3}$). Equations were developed to relate the following terms: the weight ratio (R) that was determined by dividing the observed weight by the minimum weight (reached after loss of volatile contaminants), the final weight ratio for a completely oxidized sample (R_f), the radius of an average passivated particle (r_p), the radius of a corresponding particle in an unpassivated (pure Al) state (r_{up}), and the thickness of Al oxidized (t_{Al}^{ox}). The thickness of Al oxidized in the passivated state is about 2 nm (i.e., oxidation of the outer 2 nm of a pure Al particle produces an oxide layer about 2.5 nm thick).

The radius of an average passivated particle (r_p) in nanometers can be found from the maximum weight ratio (R_f) by the equation:

$$r_p = \frac{t_{Al_2O_3}}{1 - \{1/\sqrt[3]{1 + (d_{Al}/d_{Al_2O_3}) \times [(\phi - 1)/(R_f - 1) - 1]}\}} \quad (2)$$

The factor ϕ is the stoichiometric weight ratio for converting pure Al to Al oxide (weight of Al_2O_3/weight of $2Al = 1.889$,46). For samples where complete oxidation did not occur during the standard

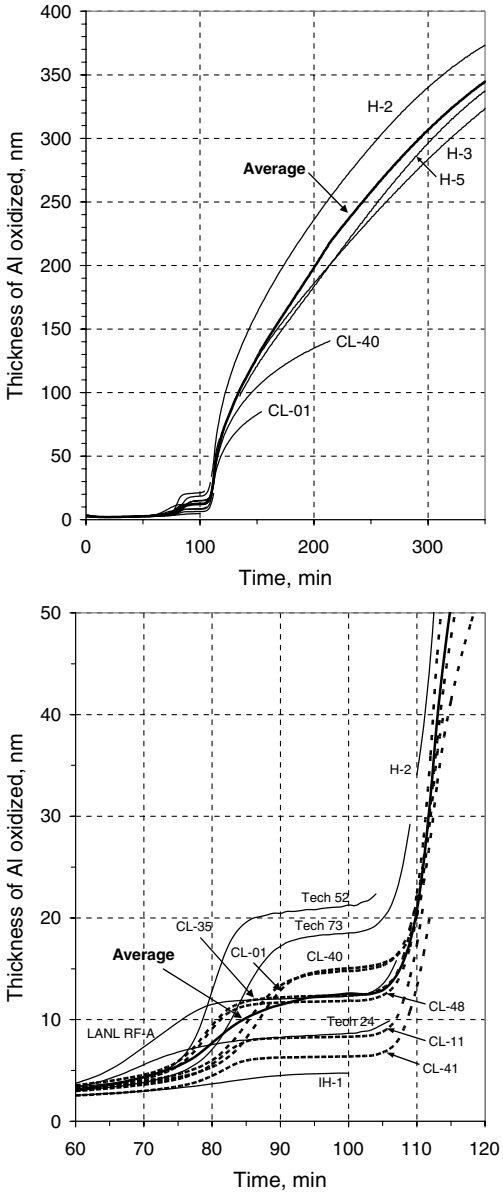

Fig. 3 TGA data plotted as the thickness of aluminum oxidized vs time. The thicker curve is the averaged data. The lower figure shows an expanded view of data at 60–120 min.

TGA experiment (where samples were held at 850°C for 4 h), the following procedures were used to determine r_p: for CL-40 the sample was held at 850°C for 16 h to give a stable final weight; for H-2, H-3, and H-5, the nominal size was used to set r_p as 1, 1.5, and 2.5 μm, respectively. The radius of a theoretical unpassivated particle in which the Al_2O_3 has been converted to Al (r_{up}) was then calculated for each sample using the value for r_p determined above:

$$r_{up} = \sqrt[3]{\frac{d_{Al_2O_3}}{d_{Al} \times \phi \times \left(r_p^3 + \{[(d_{Al} \times \phi)/d_{Al_2O_3}] - 1\} \times (r_p - t_{Al_2O_3})^3\right)}} \tag{3}$$

The thickness of the original Al that has been converted to Al_2O_3 was calculated at each point from the weight ratio curve:

$$t_{Al}^{ox} = r_{up} \times (1 - 1.2855 \times \sqrt[3]{1 - R/R_f}) \tag{4}$$

The factor 1.2855 derives from $\sqrt[3]{\phi/(\phi - 1)}$.

The master curve was calculated as the average of the empirical curves of thickness of Al oxidized vs time. Before averaging, the portions of the empirical curves corresponding to the upper and lower 5 wt% were removed. The beginning of each curve was weighted by the factor (time − time at 5 wt%)/5 for the points within 5 min of the lower 5 wt% time. Thus, the point at 5 wt% received a weight of 0, the point 1 min ahead received a weight of 0.2 until a weight of 1.0 was reached. The ending of each curve was treated similarly, except that the final 10 min was weighted. This weighting was necessary to avoid discontinuities in the averaged curve.

An average was thus compiled from all the input curves (Fig. 3). This curve was converted into a set of calculated basis curves (weight ratio versus time) in the following manner. A vector of radii was assumed (10, 20, 50, 75, 100, 250, 500, 750, and 1500 nm). A final weight ratio (R_f) was found for each passivated radius (r_p) from a rearranged version of Eq. (2):

$$R_f = 1 + (\phi - 1) \times \left\{1 + \left(\frac{d_{Al_2O_3}}{d_{Al}}\right)\left[\left(\frac{r_p}{r_p - t_{Al_2O_3}}\right)^3 - 1\right]\right\}^{-1} \tag{5}$$

The unpassivated radius was found by the same equation previously used [Eq. (3)]. The thickness of Al oxidized was converted into weight ratio by rearranging Eq. (4), and normalizing each calculated basis curve:

$$R = R_f \times \left[1 - \left(\frac{(1 - t_{Al}^{ox}/r_{up})}{1.2855}\right)^3\right] \tag{6}$$

An experimental curve to be fitted is first corrected for instrumental background and converted to weight ratio (sometimes referred to as weight fraction), and then smoothed and interpolated so that it has the same time scale and intervals as the basis curves. The proportion of each calculated basis curve in the fitted curve is then varied so that the square of the error between the calculated curve and the input curve is minimized.

Results and Discussion

Aluminum Powders and Microscopy

The aluminum powders characterized in this work originated from four distinct preparation processes: solution, electroexplosion, vapor condensation, and gas atomization. All of the methods are capable of producing a range of particle sizes, but the first three methods readily produce nanosized particles, whereas gas atomization produces mainly micron-sized and larger particles. Figure 4 shows micrographs from scanning electron microscopy (SEM) of representative powders. Particle size and morphology from SEM data are collected in Table 1. The most common particle size from visual inspection is given in Table 1, along with the range of sizes observed. For samples with broad size distributions where there is no single typical particle size, Table 1 lists an approximate size in the middle of the distribution for the most common particle size (e.g., ~250 nm for Tech 455). The solution and vapor condensation processes can give a narrow particle size range, often varying by a factor of about 3. The particle size generally varies by a factor of 20 or more for the electroexplosion and gas atomization processes. Powders prepared by the solution process tend to be tightly agglomerated into microscopic clumps, with the larger sizes exhibiting particles that are fused together (see micrographs for CL-40 and CL-57 in Fig. 4). The other three methods generally produced more loosely agglomerated particles.

Thermogravimetric Analysis in Air and Oxygen

Figures 5 and 6 show TGA data in air for some of the powders. All of the powders show an initial weight loss due to loss of volatile components (e.g., water and organic compounds) upon heating to about 350°C. Each TGA curve is normalized to the minimum weight that was reached between the weight loss due to volatiles and the weight gain due to Al oxidation. The oxidation proceeds in two distinct steps separated by slow oxidation from about 600 to 700°C. The melting of Al at 660°C appears to have no immediate effect on

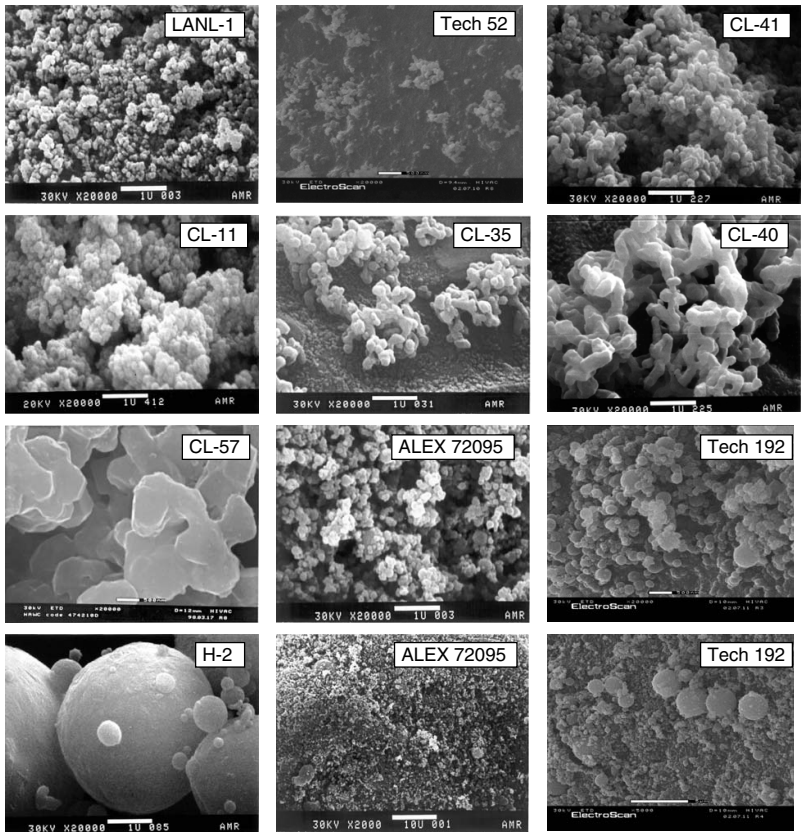

Fig. 4 SEM micrographs of aluminum powders. All of the micrographs are at the same magnification except for the last two micrographs, which show larger particles in the ALEX 72095 (bar = 10 μm) and Tech 192 (bar = 5 μm) samples. The dark fine-grained background areas in micrographs of Tech 52, CL-35, and CL-40 are part of the mounting stub surface.

the oxidation rate (see Fig. 6 for an expanded view in this region). The oxidation rate increases above 700°C, reaching a maximum between 750 and 850°C. Submicron powders are completely or nearly completely oxidized after several hours of heating at 850°C. Complete oxidation is indicated by reaching a constant weight and by the color of the residue, which is bright white when oxidation is complete, but usually noticeably gray if a small amount (about 1–2%) of unoxidized Al remains. The weight gained in the first step depends markedly on the particle size, with the smallest powders giving the largest weight gain below 700°C.

Ignition of aluminum nanopowders can readily occur in TGA experiments due to the high reactivity of the smaller powders and the high exothermicity of the oxidation reaction [24,38]. High heating rates and large samples sizes facilitate self-heating and runaway oxidation [39] of the aluminum powder. Figure 6 shows typical profiles for controlled oxidation and runaway oxidation of sample CL-B. Runaway oxidation initiated at 588°C (solid curve in Fig. 6), with about a tenfold increase in peak oxidation rate compared with the controlled oxidation case (dashed curve). Additional characteristics of the runaway oxidation are an abrupt decline in oxidation rate after the rate peaks, and subsequent sluggish oxidation at higher temperatures (in this case leaving a gray residue after several hours of heating at 850°C). This profile for runaway oxidation matches data in some literature reports [23,40–43], including a case of ignition identified for an aluminum flake sample [43]. Runaway oxidation can be avoided and the effects of self-heating minimized by using

Table 1 Characterization of aluminum powders by SEM and XRD

Sample	SEM size (range), nm	Particle morphology	XRD size, nm
Valimet H-2	—— (200–8000)	Loosely agglomerated	580
CL-57	1000 (800–1500)	Highly fused	140
CL-40	300 (150–400)	Highly fused	105
CL-01	300 (150–350)	Highly fused	104
Tech 455	~250 (50–5000)	Agglomerated	——
CL-06	250 (100–350)	Highly fused	109
Tech 192	~200 (50–3000)	Agglomerated	——
CL-35	200 (125–300)	fused	120
ALEX 72095	~150 (50–5000)	Loosely agglomerated	173
CL-41	150 (70–200)	Agglomerated	70
CL-48	125 (75–250)	fused	93
CL-11	120 (100–200)	Agglomerated	68
CL-49	120 (60–200)	Agglomerated	67
CL-10	~100 (50–300)	Highly fused	62
CL-96	100 (80–150)	Agglomerated	72
Tech 52	70 (~40–100)	Loosely agglomerated	——
LANL RF-A	60 (~40–100)	Loosely agglomerated	40
Tech 24	40 (~30–100)	Loosely agglomerated	——

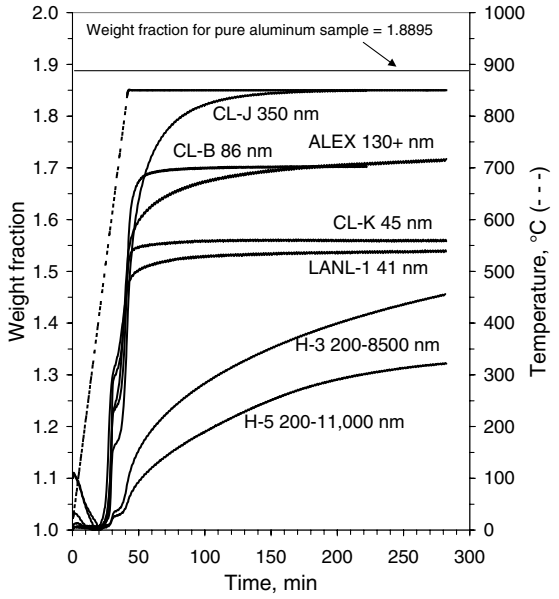

Fig. 5 TGA of aluminum powders oxidized in air. Samples were heated at 20°C/min to 850°C, then held at 850°C for 4 h. The sample weight was normalized to the minimum weight.

very small sample weights with the powder well spread out in the pan, or by lowering the heating rate. However, if the sample size is large for a highly reactive powder, ignition can still occur at a 3°C/min heating rate, as shown in Fig. 7 for Al powder CL-11, which is similar in particle size to CL-B. In this case runaway oxidation initiated at 525°C, and the peak oxidation rate increased 100-fold, giving a large spike in the temperature recorded by a thermocouple located a couple of millimeters away from the sample. Analysis by x-ray diffraction of a TGA residue after ignition (from a 34-mg sample of CL-11) showed intense peaks for Al nitride and Al oxide, consistent with a previous report [44], along with weaker peaks for an Al oxynitride phase (either $Al_{2.78}O_{3.65}N_{0.35}$ or $Al_{2.81}O_{3.56}N_{0.44}$) and Al metal.

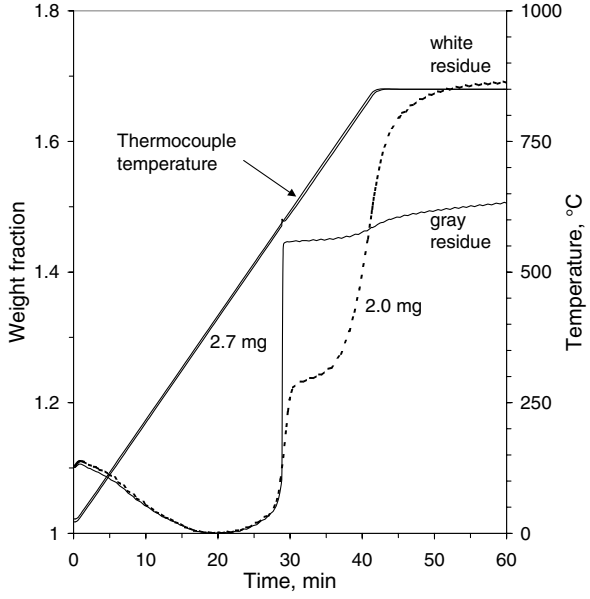

Fig. 6 TGA of aluminum powder CL-B (∼80 nm) in air showing controlled oxidation (dashed line, 2.0 mg sample) compared with runaway oxidation (solid line, 2.7 mg sample). Samples were heated at 20°C/min to 850°C, then held at 850°C. The sample weight was normalized to the minimum weight.

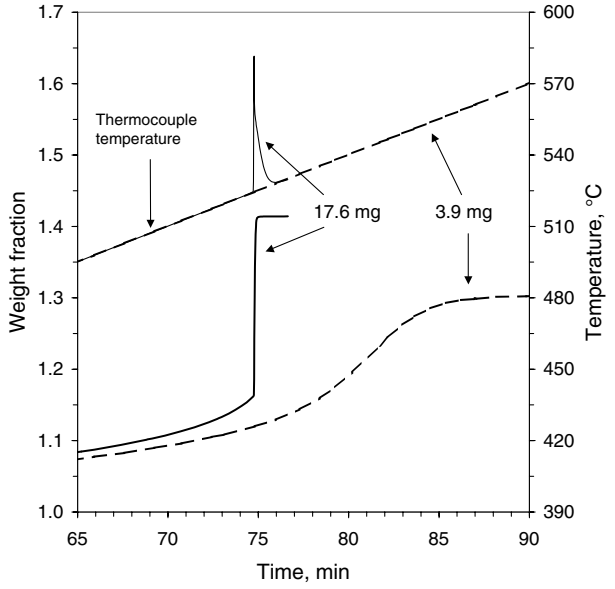

Fig. 7 TGA of aluminum powder CL-11 in air showing runaway oxidation (solid line, 17.6 mg sample) compared with controlled oxidation (dashed line, 3.9 mg sample). Samples were heated at 3°C/min after an initial ramp at 20°C/min to 350°C. The sample weight was normalized to the minimum weight, which was 98.1% of the initial weight.

Runaway oxidation was also observed for ALEX Al when a 10-mg sample was heated at 25°C/min. The final weight gain after heating at 1050°C for 1000 min was only 57%, compared with a 75% weight gain for material heated to 950°C for 240 min where runaway oxidation did not occur (4 mg sample with a heating rate of 3°C/min in the range of 350–600°C). In this case the reduced weight gain was mainly attributed to incomplete oxidation of Al, rather than extensive nitridation, because the x-ray diffraction pattern showed intense Al oxide peaks, medium intensity Al metal peaks, and weak peaks for Al nitride. Our results on the products of runaway oxidation qualitatively match a report where smaller quantities of nano-Al ignited to give $\alpha - Al_2O_3$, residual Al, and trace quantities of nitride, whereas larger sample weights reached higher temperatures and produced more nitride at the expense of both residual Al and $\alpha - Al_2O_3$ [45].

If complete conversion of the metallic aluminum to Al_2O_3 occurs in the TGA experiment, then the weight gain can be used to calculate the weight percent of active Al originally present in the sample. For this calculation the samples are assumed to consist of only unreacted Al and Al oxide at the point of minimum weight. The subsequent weight gain is ratioed to the theoretical weight gain of pure Al converting to Al_2O_3, where the weight increases by 88.95% [i.e., weight fraction of active Al $= (R_f - 1)/(\phi - 1)$]. The weight changes for the Al samples are listed in Table 2 (columns 2 and 3), along with the calculated weight percent of active Al (column 4).

To check for the possibility that nitridation occurs during the controlled oxidation of Al in air, TGA was conducted in pure oxygen. Figure 8 shows TGA curves of sample CL-35 heated in air and oxygen. The TGA curves are identical, and so there is no evidence for nitridation during heating in air. Conversion of Al to AlN results in a weight increase of only 51.91%, compared with 88.95% for Al_2O_3. Because the weight gains under air and oxygen are the same throughout the oxidation process, the rate of oxidation is the same in air and pure oxygen.

The weight percent active Al was also determined by hydrolysis of the Al, with quantitative determination of the gas evolved. The results are listed in Table 3, with the corresponding values from TGA data listed for comparison. The TGA values in Table 3 are based on the material "as is," that is, before loss of volatiles during heating, and therefore differ slightly from the values in Table 2. Excellent agreement between the two methods is found for seven samples, whereas the three smaller China Lake powders gave lower active

Table 2 Characterization of aluminum powders by TGA and the BET

Sample[a]	% volatiles[b]	% weight gain[c]	Weight % active Al[f]	TGA size, nm	Surface area, m^2/g	BET size, nm	% weight gain in N_2 (expected)
Valimet H-5, M	0.4	31.4[d]	——	——	——	——	——
Valimet H-3, M	0.3	46.0[d]	——	——	——	——	——
Valimet H-2, M	0.2	78.2[d]	——	——	2.14	1035	48.5 (51.3[h])
CL-57	1.6	60.26[d]	——	——	——	——	——
Tech 455	0.5	66.69[d]	——	——	5.2	430	——
CL-40, M	0.4	84.77[e]	95.3	460	6.9	322	42.8 (49.5)
CL-J	0.5	83.60	94.0	355	——	——	——
CL-01, M	1.8	81.64	91.9	256	10.6	209	26 (47.7)
Tech 192	1.1	73.30[d]	——	——	11.7	190	——
CL-35, M	1.7	79.75	89.6	201	15.7	141	55 (46.5)
CL-06	1.9	79.27[e]	89.1	190	——	——	——
ALEX 72095	1.1	75.12[d]	>84.5[d]	>130[d]	13.3	167	47 (45.1[h])
CL-48, M	2.2	75.84	85.3	138	——	——	——
CL-10	3.1	70.24	79.0	93	——	——	——
Tech 73, M	2.6	69.86	78.5	90	28.4	78	——
CL-B	10.4	69.04	77.6	86	——	——	——
CL-11, M	1.9	65.93	74.1	73	55.4	40	43 (38.5)
CL-96	6.2	64.32	72.2	67	53.6	41	47 (37.5)
Tech 52, M	2.9	63.98	71.9	66	39.0	57	——
CL-41, M	5.5	63.04	70.9	63	79.0	28	40.4 (36.8)
LANL RF-A, M	4.3	56.98	64.0	49	48.1	46	43.2 (33.2)
CL-K	10.4	54.59	61.4	45	——	——	——
LANL-1	3.7	52.40	58.9	41	——	——	——
LANL RF19	4.1	46.16	51.9	33	——	——	——
Tech 24, M	3.6	41.08	46.2	28	69.6	32	——
CL-49	20.9	33.77	39 ± 2[g]	~23	51.2	43	——
IH-1, M	10.0	19.93	22.4	15	——	——	——

[a]TGA data from the 14 samples with M following the name were used in generating the master curve that was used for TGA curve-fitting analysis.
[b]The percent volatiles is the percent weight loss from the initial weight to the minimum weight reached at 300–350°C.
[c]The percent weight gain is computed from the final weight (typically after 4 h at 850°C) and the minimum weight. Unless otherwise noted, samples were heated according to the following program: 20°C/ min to 350°C, 3°C/ min to 600°C, 20°C/ min to 850°C, hold 4 h at 850°C. For the data in this table, samples CL-J, CL-B, CL-K, LANL-1, and LANL RF19 were heated at 20°C/ min to 850°C, then held for 4 h at 850°C.
[d]Oxidation incomplete. The H-2 sample was heated for 8 h at 850°C and 2 h at 950°C (after 4 h at 850°C, the weight gain was 61.02%). The ALEX sample was heated for 4 h at 950°C to give nearly complete oxidation (after 4 h at 850°C, the weight gain was 70.85%).
[e]Sample CL-40 was heated for 16 h at 850°C to give complete oxidation (after 4 h at 850°C, the weight gain was 83.43%). Sample CL-06 was heated for 8 h at 850°C to give complete oxidation (after 4 h at 850°C, the weight gain was 78.66%).
[f]The weight % of active Al listed here is for the material remaining after volatile components are lost.
[g]Sample contains ~10 mole % Ti impurity. The total active metal content is given here and depends on the form of the Ti (i.e., Ti metal or TiO_2).
[h]Based on the weight % active Al determined by base hydrolysis.

metal contents by the TGA method. For the ALEX powder, the active metal content from hydrolysis, 86.0%, is close to the TGA result of >83.6%, where the oxidation was not quite complete (the residue had a dull white coloration).

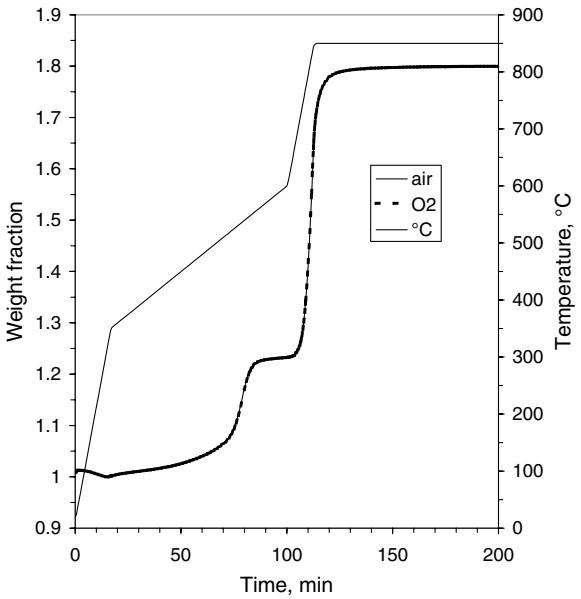

Fig. 8 TGA of aluminum powder CL-35 undergoing oxidation in air and oxygen atmospheres.

Surface Area Measurement and Particle Size Determinations by TGA

Surface area measurements are widely used to provide a measure of average particle size of nano-Al powders. Typically, the particle size calculation is based on the assumption of monosized spherical particles. Specific surface area results obtained from gas adsorption are listed in Table 2, along with the BET average particle size (particle diameter $= 2r$) in nanometers calculated using the equation $A_s = 3000/(r \times d_{Al})$, where the specific surface area A_s is in m^2/g,

Table 3 Comparison of weight percent of active aluminum metal as determined by the hydrolysis method and by the TGA method

Sample	Weight % Al, hydrolysis	Weight % Al, TGA[a]
Valimet H-2	98.7	——
Tech 455	94.9	——
CL-40	94.5	94.9
Tech 192	89.8	——
ALEX 72095	86.0	>83.6
CL-48	84.0	83.4
CL-10	80.7	76.6
Tech 73	77.6	76.5
CL-41	72.1	67.0
Tech 52	71.6	69.9
LANL RF-A	61.8	61.2
Tech 24	46.2	44.5
CL-49	35.1	31 ± 2[b]

[a]Weight % Al was calculated for the samples "as is," that is, before loss of volatiles.
[b]Sample contains ~10 mole % Ti impurity. The total active metal content is given here and depends on the form of the Ti (i.e., Ti metal or TiO_2).

and the density of particles was taken to be the density of Al, 2.702 g/cm^3, without correction for a different density in the oxide layer. The BET average particle sizes are within the size range obtained by SEM (see Table 1) for most samples.

Just as surface area data provide a useful indirect measure of particle size, TGA data can be similarly interpreted if oxidation of the Al powder is complete. The weight gain upon complete oxidation of the Al was used to calculate a weight-averaged particle size using Eq. (2). For simplicity in this calculation the powders were assumed to have an oxide coating equivalent to 2.5 nm of fully dense α–Al_2O_3 ($d = 3.965$ g/cm^3). (In [20], an oxide thickness of 3.68 nm was used for calculating particle sizes from TGA data, instead of the currently preferred value of 2.5 nm. The TGA sizes in [20] can be converted by multiplying by 2.5/3.68.) Reported values for the thickness of the native oxide layer on Al exposed to air range from about 2 to 4 nm [9,10,15,28,46–49]. The density of the Al oxide passivation layer is actually less than 3.965 g/cm^3; however, the exact density varies between samples. The calculated TGA sizes represent a weight- or volume-weighted average particle size. Inspection of Eq. (2) shows that the calculated TGA size is directly proportional to the assumed oxide thickness. The TGA particle sizes are shown in Fig. 5 and in column 5 of Table 2. The TGA particle sizes are generally consistent with the SEM particle sizes shown in Table 1. The data in Table 2 show that the active Al content drops rapidly as the particle size falls below 100 nm (e.g., 52% active Al for 33 nm particles). For energy producing applications a tradeoff exists between enhanced reactivity and reduced energy content. This tradeoff could be mitigated by using unpassivated submicron Al powders, which are pyrophoric, or possibly by developing alternatives to oxide passivation of the Al [20,33].

Particle size data from BET, SEM, and TGA data are presented graphically in Fig. 9, along with average crystallite sizes determined by x-ray diffraction. The TGA and BET sizes correlate very well, with the TGA size generally slightly larger than the BET size. This confirms that the TGA method gives a useful measure of particle size. The fit between TGA size and BET size could be improved somewhat by adjusting the oxide thickness and density, however, the differences may reflect other factors than size, such as surface roughness, or porosity in the oxide passivation layer. The TGA and BET sizes show a fair correlation with the SEM sizes. Assigning a single particle size based on SEM micrographs is somewhat subjective, and complicated by the agglomeration of particles, the distribution of particle sizes, and the image resolution limitations for particle sizes below 100 nm. The average crystallite size correlated well with particle sizes for the LANL and ALEX materials. For the China Lake samples, the crystallite size exhibited a much narrower range than the particle sizes. The results indicate that in the smaller size powders many of the particles are single crystals, whereas the larger size materials generally contain polycrystalline particles. The polycrystalline particles could form by secondary nucleation occurring on the particle surface, or by many separate particles aggregating and growing together.

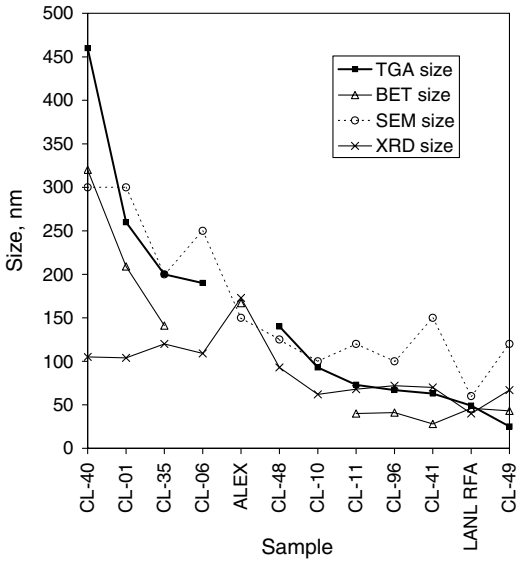

Fig. 9 Comparison of particle and crystallite sizes obtained from TGA, BET, SEM, and XRD analysis.

Curve Fitting of TGA Data to Examine Particle Size Distribution

In TGA experiments with Al powders, the shape of the weight gain curve is affected by both particle size and particle size distribution. This section describes attempts to extract particle size distribution information from the TGA data by summing together experimental or calculated TGA curves for various sizes of Al. Details on the curve-fitting procedures are given in the Experimental Methods section.

Curve Fitting with Empirical Basis Curves

The initial approach involved the fitting of an experimental curve of a sample with a broad size distribution by summing together a set of experimental curves of samples with relatively narrow size distribution (these curves are shown in Fig. 2). Qualitative information on size distribution is available from examination of SEM micrographs and visual inspection of the TGA curves, based on experience with correlating SEM and TGA results. For example, samples containing micron-sized aluminum particles continue to gain weight after 4 h at 850°C, whereas samples containing mainly particles ≤ 50 nm show nearly complete oxidation below the melting point of aluminum (660°C). A sample containing predominantly small particles (Tech 73 in Fig. 2) oxidizes more extensively at low temperature, with a relatively small overall weight gain at the completion of oxidation due to a high proportion of aluminum oxide present as the passivation layer. A sample containing predominantly large particles shows little weight gain at relatively low temperature, and a sluggish weight increase at high temperature.

Aluminum powder sample Tech 192 was chosen for curve-fitting analysis based on the broad size distribution evident by SEM (see Fig. 4 and Table 1). Sample Tech 192 is nominally 192 nm based on surface area analysis, and the oxidation curve was fit by combining the curves from samples nominally 90 nm ("Tech 73"), 200 nm ("CL-35"), 460 nm ("CL-40"), 2000 nm ("H-2"), 3000 nm ("H-3"), and 5000 nm ("H-5"). Figure 10 shows the experimental and calculated curves, along with a histogram showing the makeup of the calculated curve. Overall, there is excellent agreement between the Tech 192 curve and the combined curve from the basis set samples. This result supports the notion that the TGA curve represents the sum total of the oxidation behavior of essentially independently reacting particles.

Although the oxidation was not complete for the Tech 192 sample, the active Al content can still be estimated by using the active Al contents of the samples used in the curve fit. The calculated value was 88.7%, which agrees well with the experimental value of 89.8% determined volumetrically by base hydrolysis. Based on 89.8% active Al content, the weight fraction curve in Fig. 10 would reach 1.798 at complete oxidation.

Curve Fitting with Calculated Basis Curves

Efforts were next directed to deriving a more detailed particle size distribution by developing calculated basis curves for specified sizes of Al particles. This approach relies upon a model of Al oxidation where the reaction proceeds uniformly inward from the exterior of spherical particles, such that the thickness of the original layer of Al that has been converted to oxide at any point in time is the same for different size particles. Thus, the weight vs time data were converted to thickness of Al oxidized vs time for each experimental curve, as described in the Experimental Methods section (see Fig. 3) [50]. The resulting curves were then averaged to give a master curve of thickness of Al oxidized vs time (also shown in Fig. 3). Note that the

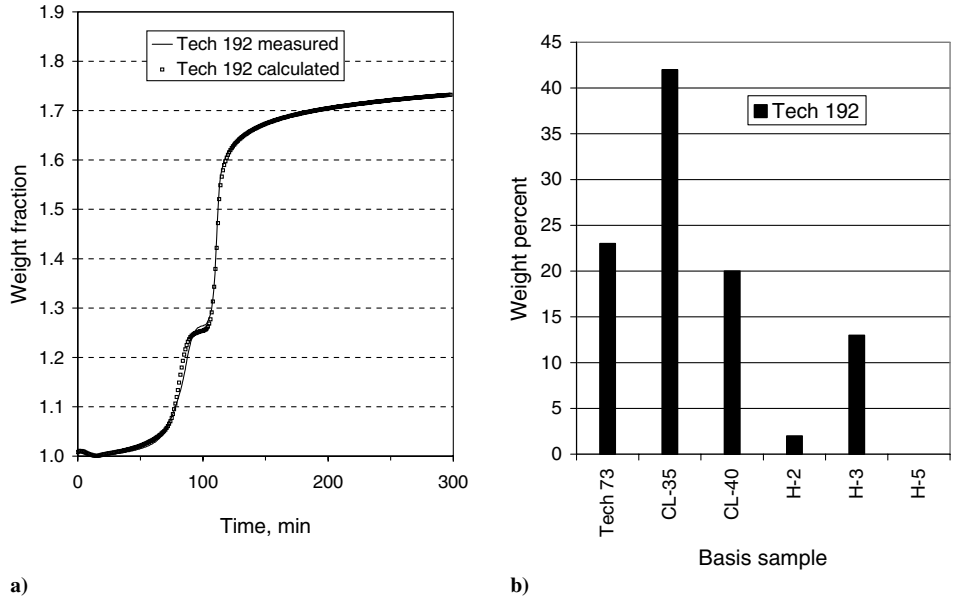

a) b)

Fig. 10 Curve fit using empirical basis curves for Tech 192 aluminum powder: a) plot of experimental and calculated curves; b) histogram of the curve fit showing the basis samples.

experimental curves in Fig. 3 were truncated slightly to reduce the effects of the outer parts of the size distributions on the shape of the master curve. From the master curve, TGA curves were calculated for particle diameters of 20, 40, 100, 150, 200, 500, 1000, 1500, and 3000 nm.

Many of the experimental curves deviate considerably from the master curve in Fig. 3. Before describing the curve-fitting results, some comments are in order regarding the shape of the master curve and the variations of the experimental curves. The flat part of the thickness of Al oxidized curves in the region around 100 min (where the temperature is about 600°C, see Fig. 3) is related to the formation of a "barrier" oxide layer, which has been studied for flat pieces of Al [51–53]. Typical values for the barrier oxide thickness are 17–21 nm from studies of smooth flat surfaces at 500–600°C [51]. This oxide thickness would correspond to an Al thickness oxidized of roughly 15 nm, which is about the middle of the observed values in Fig. 3 (see the expanded view where most samples are in the range of 8–20 nm for thickness of Al oxidized at 100 min). In agreement with these results, estimated oxide thicknesses of 14–20 nm were recently reported for micron-sized aluminum powders heated to 650°C, based on TGA weight gains [43]. Another report estimated an oxide layer thickness of only 6–10 nm for oxidation below 627°C, but this thickness may be biased by a low particle size used in the calculation [30].

Variations between the individual curves in Fig. 3 may indicate differences in reactivity or incorrect assumptions in the simple model for the oxidation process. Differences in reactivity may relate to differences in chemical composition or morphology. The CL samples contain titanium that originates from the catalyst used in the synthesis process. In Fig. 11, a plot of the thickness of aluminum oxidized at 600°C vs the amount of titanium catalyst shows that the oxidation in the first step becomes strongly inhibited as the amount of titanium catalyst is increased from 0.1 to 10%. Note that the thickness of aluminum oxidized before heating is already about 2 nm from air passivation. Before this analysis, we had considered sample CL-49 (prepared using 10% titanium catalyst) to be an unexplained "outlier," due to its nearly nonexistent first oxidation step, yet small particle size (43 nm by BET). An inhibiting effect of titanium on the oxidation of Al below 660°C has also been observed for Ti-Al mechanical alloys [54].

The CL samples exhibit a relatively high degree of particle agglomeration, with considerable necking between particles for the larger sizes. This fusing of particles may be responsible for the CL-40 and CL-01 curves dropping away from the master curve in Fig. 3 in the latter stages of the reaction. In addition, there may still be an inhibiting effect of titanium, even though these samples contain only about 0.1% Ti.

Some of the observed variations in Fig. 3 may result from inaccurate particle sizes or excessively broad size distributions. For the H-2, H-3, and H-5 samples, the true average size may vary from the nominal size used in the analysis. For example, the BET size of H-2 was 1.0 μm (Table 2). Reducing the particle size would lower the corresponding curve in Fig. 3. The smallest samples, Tech 24 and IH-1, have low values for the thickness of Al oxidized near 600°C, which could be due in part to larger particles in the samples.

Curve fitting with the calculated basis curves gave the results shown in Fig. 12 for sample Tech 192. The curve fit result is comparable to that in Fig. 10, where experimental basis curves were used for fitting (the variance for the curve fit in Fig. 12 is 0.000,06, whereas the variance for the curve fit in Fig. 10 is 0.000,05). The

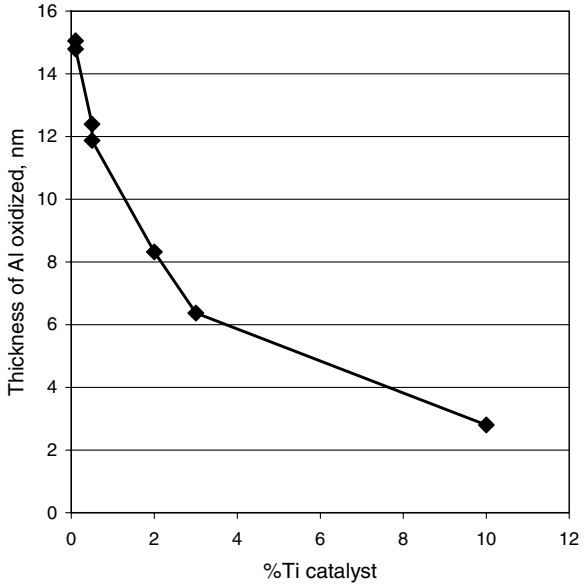

Fig. 11 Plot of the thickness of aluminum oxidized calculated from the weight gain upon heating powders to 600°C vs the amount of titanium catalyst used in the synthesis.

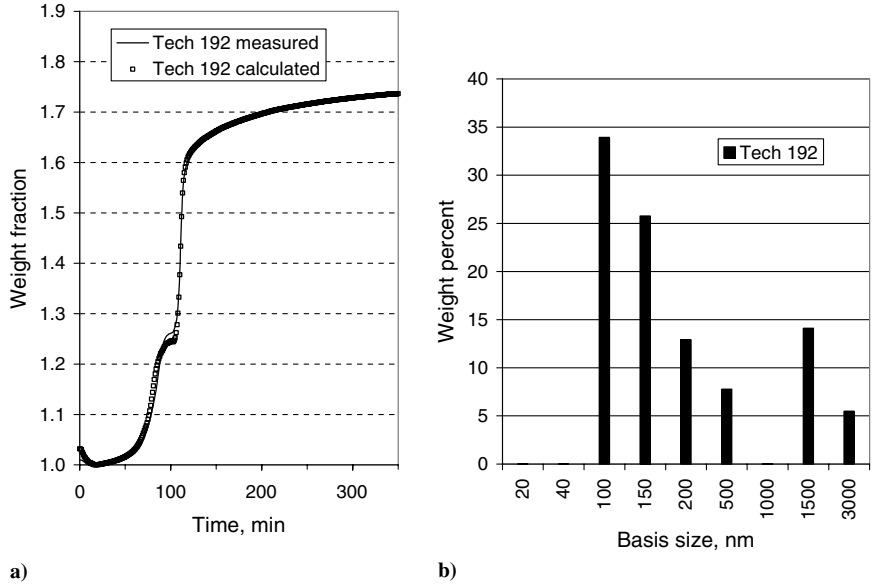

Fig. 12 Curve fit using calculated basis curves for Tech 192 aluminum powder: a) plot of experimental and calculated curves; b) histogram of the particle size distribution showing the basis curve sizes.

histogram of the size distribution in Fig. 12b shows a broad distribution of particle sizes from 100 to 3000 nm in diameter. This distribution matches well with the SEM micrographs in Fig. 4 that clearly show a broad range of particle sizes up to about 3000 nm in diameter. Apparent discrepancies are the lack of any contribution from the 40 and 1000 nm basis curves, although, on a weight basis the fraction of 40 nm particles is very small. From the histogram results, the calculated active Al content for Tech 192 is 87.9%, which compares to 88.7% for the empirical curve-fitting analysis (Fig. 10), and 89.8% from base hydrolysis analysis.

The curve fit and histogram for the ALEX Al powder are shown in Figs. 13. The histogram indicates that, whereas particle sizes are concentrated near 150 nm, roughly 20% of the material consists of micron-sized particles. Scanning electron micrographs reveal these micron-sized particles, as shown in Fig. 4 (picture taken at 2000X magnification), giving qualitative agreement with the histogram results. The size distribution for this material is distinctly not monomodal, in agreement with a literature report mentioning a bimodal distribution with maxima in the regions of 100 and 1000–3000 nm for a similar electroexploded powder [8]. Broad size distributions with coarse particles are reported to be inherent for the exploding wire method [12]. The curve fit in Fig. 13a is rather poor for the first 30% weight gain, with the sample appearing to react sluggishly for the first 20% weight gain. This behavior appears to be unique for the electroexploded powders, and results in the absence of 100 nm particles in the histogram, despite their obvious abundance from electron micrographs.

Curve fits were also conducted for most of the 14 samples used to generate the master curve (excluding the largest and smallest samples). Table 4 lists the results for the curve fits, including the variance between the calculated and experimental curves. Also included in Table 4 are mean particle sizes calculated from both the area distribution (D[3,2]) and volume distribution (D[4,3]), along with the TGA particle sizes copied from Table 2. The volume mean diameter is weighted toward large particles, and so this size is much larger than the area mean diameter when the curve fit indicates the presence of relatively large particles in the sample. The area mean particle sizes agree very well with the TGA sizes, consistent with the

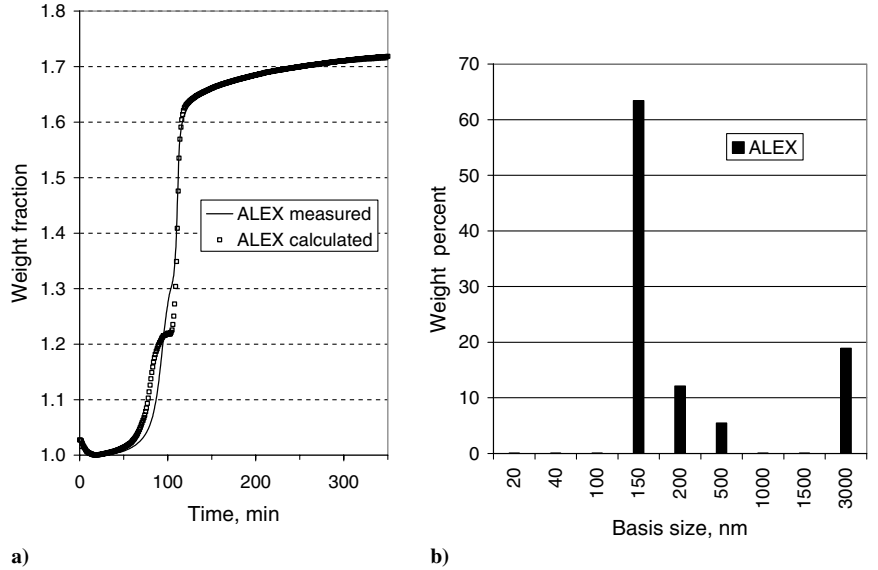

Fig. 13 Curve fit using calculated basis curves for ALEX aluminum powder: a) plot of experimental and calculated curves; b) histogram of the particle size distribution showing the basis curve sizes.

Table 4 Particle size distribution results from curve fits using nine calculated basis curves

Sample	Mean size, $D[3,2]$ nm[a]	Mean size, $D[4,3]$ nm[b]	TGA size, nm	20	40	100	150	200	500	1000	1500	3000	Variance
H-2	817	1823	——	0.00	0.02	0.01	0.00	0.00	0.08	0.00	0.59	0.30	0.00001
CL-40	402	559	460	0.00	0.00	0.01	0.00	0.20	0.59	0.16	0.05	0.00	0.00004
CL-01	246	334	256	0.00	0.00	0.10	0.00	0.42	0.48	0.00	0.00	0.00	0.00015
ALEX	199	715	>130	0.00	0.00	0.00	0.63	0.12	0.05	0.00	0.00	0.19	0.00051
CL-35	189	193	201	0.00	0.00	0.00	0.16	0.84	0.00	0.00	0.00	0.00	0.00007
Tech 192	166	514	——	0.00	0.00	0.34	0.26	0.13	0.08	0.00	0.14	0.05	0.00006
CL-48	126	135	138	0.00	0.00	0.40	0.55	0.03	0.01	0.00	0.00	0.00	0.00006
Tech 73	91	97	90	0.00	0.07	0.93	0.00	0.00	0.00	0.00	0.00	0.00	0.00206
CL-11	67	152	73	0.15	0.00	0.54	0.29	0.00	0.00	0.00	0.00	0.02	0.00012
Tech 52	62	77	66	0.00	0.40	0.59	0.00	0.00	0.00	0.00	0.00	0.00	0.00419
CL-41	60	267	63	0.24	0.00	0.00	0.71	0.00	0.00	0.00	0.00	0.05	0.00029
LANL RF-A	46	54	49	0.00	0.79	0.21	0.00	0.00	0.00	0.00	0.00	0.00	0.00168
Tech 24	28	32	28	0.45	0.55	0.00	0.00	0.00	0.00	0.00	0.00	0.00	0.00031

[a]Mean diameter of the area distribution, calculated as $(\Sigma V_i)/[\Sigma(V_i/d_i)]$, where V_i is the volume fraction for each basis size, and d_i is the basis size.
[b]Mean diameter of the volume distribution, calculated as $(\Sigma V_i d_i/\Sigma V_i)$.

area-weighted nature of the TGA size, and the fact that both sizes are determined from TGA data.

The curve fit for sample Tech 52, shown in Fig. 14a, exhibited the largest variance. This sample oxidizes more extensively in the first step than expected based on the master curve (see Fig. 3). This is partly due to the master curve being suppressed by the inhibiting effect of titanium on the oxidation of the CL samples. Although the curve fit was poor for Tech 52, the size distribution was not unreasonable, giving 40% of 40 nm and 59% of 100 nm. Similar reactivity effects account for the high variances for the curve fits of Tech 73 and LANL RF-A.

For samples CL-41 and CL-11, where the oxidation is strongly inhibited by titanium, the curve fit tries to account for the smaller than expected weight gain in the first step by distorting the size distribution to include both very large and very small particles. Figure 14b shows the curve fit for sample CL-41, which was prepared using 3% Ti. Large particles in the calculated curve for CL-41 lead to weight gains at longer times, whereas the experimental curve is flat at longer times, indicating that large particles are not present in this sample (this is also confirmed by the SEM analysis, as illustrated by the micrograph in Fig. 4).

Thermogravimetric Analysis in Nitrogen

The nitridation of Al powders was studied isothermally at 600°C by TGA. Figure 15 displays results of TGA experiments under nitrogen for the current group of powders. The maximum weight gain is given in the last column in Table 2, along with the expected maximum weight gain, based on the active metal content. The most surprising result is the rapid and nearly complete nitridation of the H-2 powder, shown in Fig. 15a. For comparison, in air H-2 Al gained only 7 wt % upon heating at 600°C for 900 min. Thus, for H-2 Al the Al nitride product does not significantly inhibit nitridation at 600°C, unlike the strong inhibiting effect of Al oxide. The second largest powder studied, CL-40 (TGA size 460 nm), also exhibited rapid and extensive nitridation. In contrast, the third largest powder studied, CL-01 (TGA size 256 nm) was the slowest to react and gave by far the lowest maximum weight gain. The smaller powders gave somewhat scattered results, but all ultimately gave maximum weight gains that were larger than expected. Sample CL-35 was run for 28,000 min, giving a maximum weight gain of 55%, which is higher than the theoretical value of 51.9% for pure Al. These results are generally consistent with nonisothermal TGA experiments that showed rapid nitridation of Al nanopowders around 700°C [23,40].

The residues from nitridation of samples CL-41 and CL-35 were analyzed by x-ray diffraction (XRD). The diffraction pattern in Fig. 16 for the CL-41 residue shows mainly the hexagonal AlN phase, some unreacted Al, and possibly Al oxynitride phases that may be associated with weak peaks in the pattern. Amorphous Al oxide phases may also be present. The TGA and XRD results indicate that Al oxynitride or oxide phases are formed, especially at longer times in the TGA experiment. Traces of oxygen or water in the system apparently react with the Al or with the AlN product. Thermodynamics dictate that any available oxygen in the system should form Al oxide, in view of the fact that the conversion of $AlN + O_2$ to $Al_2O_3 + N_2$ is favored by 489 kJ/mol Al at 600°C,

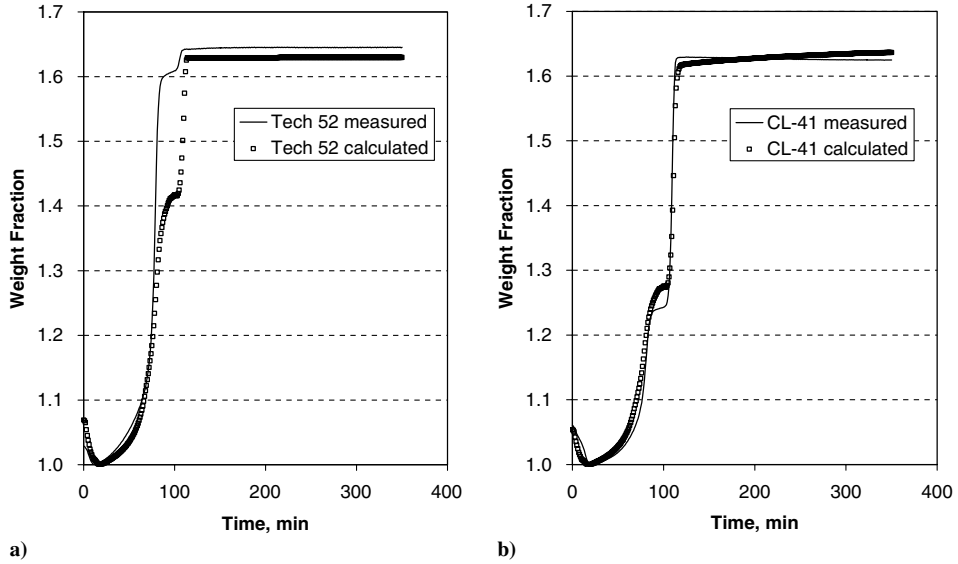

Fig. 14 TGA curves for a) Tech 52 and b) CL-41 aluminum powders along with fitted curves using calculated basis curves.

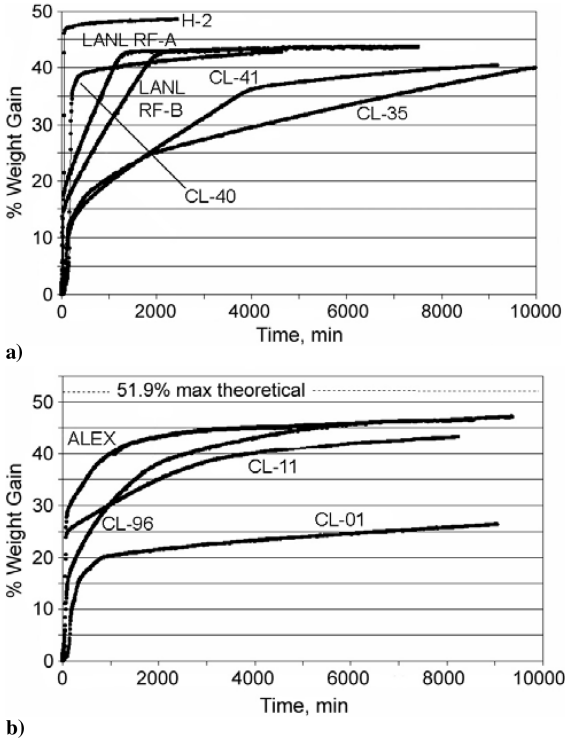

Fig. 15 TGA curves of aluminum powder reaction with nitrogen at 600°C.

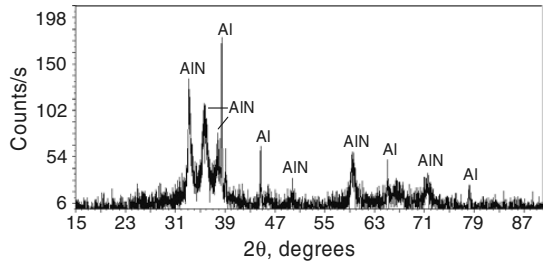

Fig. 16 X-ray diffraction of nitrided aluminum powder CL-41.

whereas the conversion of $AlN + H_2O$ to $Al_2O_3 + NH_3$ is favored by 152 kJ/mol.

Conclusions

Weight changes during thermogravimetric analysis of submicron aluminum powders in air provide quantitative information on active metal and Al oxide content, volatile impurities, and particle size. The time and temperature dependence of the Al oxidation process provides qualitative information on particle size distribution, and can also provide evidence for impurities that affect the oxidation process. Particle sizes calculated from TGA data correlate well with particle sizes derived from surface area measurement by gas adsorption. This correlation is reasonable because the weight fraction of the Al oxide passivation layer depends on the surface area of the particles. In contrast to oxidation, nitridation at 600°C proceeded with much less inhibiting effect of the Al nitride product on the reaction.

Curve fitting of TGA data provided useful information on particle size distribution for Al powders, especially for samples with a broad range of particle sizes. This method is well suited to monitoring the presence of 500–5000 nm particles within nominally nanosized samples. The size distribution results were mostly in qualitative agreement with SEM characterization. However, the curve-fitting analysis generally did not provide quantitative information about particle sizes around 100 nm or smaller, due to large variations in oxidation behavior below 700°C. One source of variation was the inhibitive effect of the titanium impurity present in samples prepared by the solution method. Better fits for the particle size distribution would likely be obtained if the sample set was limited to high purity samples prepared by vapor condensation methods.

Acknowledgments

The work at China Lake was supported by the Strategic Environmental Research and Development Program Green Missile Program, by the Office of Naval Research (J. Goldwasser, R. Carlin, and J. Chew), and by the Naval Air Warfare Center Core Science and Technology program. This work was also supported, in part, by the Propulsion Directorate of the Air Force Research Laboratory, Edwards Air Force Base. Curtis Johnson thanks Richard Scheri, Michael Dowd, Dan Kline, and John Johnson for scanning electron microscopy characterization, and Brian Zentner for synthesis of aluminum powders. We also thank Chris Aumann and Joe Martin for providing the Los Alamos National Laboratory aluminum powders and communicating unpublished results, and Pamela Carpenter for providing the Indian Head Division aluminum powder. Ismail Ismail and Tom Hawkins thank Diane Hagler, Robert Stanley, and Mark Feathers at Redstone Arsenal for their support of this work in the Strategic Environmental Research and Development Program Green Missile program. Special appreciation goes to Kevin Chaffee for the x-ray diffraction work, to Paul Jones for thermogravimetric analysis work, and to Adam Brand and Milton McKay for their technical support and stimulating discussions.

References

[1] Gurganus, T. B., "Aluminum Powder Applications," *Advanced Materials and Processes*, Vol. 148, No. 2, 1995, pp. 57–59.

[2] Kearns, M., "Development and Applications of Ultrafine Aluminium Powders," *Materials Science and Engineering A*, Vols. 375–377, July 2004, pp. 120–126.

[3] Jorgensen, B., Busse, J., Smith, B., and Son, S., "Standard Characterization of MIC Materials," Los Alamos National Laboratory, LA-14086, Los Alamos, NM, 2003.

[4] Granier, J. J., and Pantoya, M. L., "The Effect of Size Distribution on Burn Rate in Nanocomposite Thermites: A Probability Density Function Study," *Combustion Theory and Modeling*, Vol. 8, No. 3, 2004, pp. 555–565.

[5] Roy, C., Dubois, C., Lafluer, P., and Brousseau, P., "The Dispersion and Polymer Coating of Ultrafine Aluminum Powders by the Ziegler Natta Reaction," in *Synthesis, Characterization and Properties of Energetic/Reactive Nanomaterials: Materials Research Society Symposium Proceedings*, edited by R. Armstrong, N. Thadhani, W. Wilson, J. Gilman, and R. Simpson, Vol. 800, Materials Research Society, Warrendale, PA, 2004, pp. 79–84.

[6] Puszynski, J. A., "Formation, Characterization, and Reactivity of Nanoenergetic Powders," *Proceedings of the 29th International Pyrotechnics Seminar*, edited by F. J. Schelling, IPSUSA Seminars, Inc., Marshall, TX, 2002, pp. 191–202.

[7] Granqvist, C. G., and Buhrman, R. A., "Ultrafine Metal Particles," *Journal of Applied Physics*, Vol. 47, No. 5, 1976, pp. 2200–2219.

[8] Il'in, A. P., Gromov, A. A., and Yablunovskii, G. V., "Reactivity of Aluminum Powders," *Combustion, Explosion and Shock Waves*, Vol. 37, No. 4, 2001, pp. 418–422.

[9] Aumann, C. E., Skofronick, G. L., and Martin, J. A., "Oxidation Behavior of Aluminum Nanopowders," *Journal of Vacuum Science and Technology B*, Vol. 13, No. 3, 1995, pp. 1178–1183.

[10] Sanchez-Lopez, J. C., Gonzalez-Elipe, A. R., and Fernandez, A., "Passivation of Nanocrystalline Al Prepared by the Gas Phase Condensation Method: An X-Ray Photoelectron Spectroscopy Study," *Journal of Materials Research*, Vol. 13, No. 3, 1998, pp. 703–710.

[11] Baudin, G., Lefrancois, A., Bergues, D., Bigot, J., and Champion, Y., "Combustion of Nanophase Aluminum in the Detonation Products of Nitromethane," *Proceedings of the 11th International Symposium on Detonation*, Office of Naval Research 33300-5, Office of Naval Research, Arlington, VA, 1998, pp. 989–997.

[12] Ivanov, Y. F., Osmonoliev, M. N., Sedoi, V. S., Arkhipov, V. A., Bondarchuk, S. S., Vorozhtsov, A. B., Korotkikh, A. G., and Kuznetsov, V. T., "Productions of Ultra-Fine Powders and Their Use in High Energetic Compositions," *Propellants, Explosives, Pyrotechnics*, Vol. 28, No. 6, 2003, pp. 319–333.

[13] Weigle, J. C., Luhrs, C. C., Chen, C. K., Perry, W. L., Mang, J. T.,

Nemer, M. B., Lopez, G. P., and Phillips, J., "Generation of Aluminum Nanoparticles Using an Atmospheric Pressure Plasma Torch," *Journal of Physical Chemistry B*, Vol. 108, No. 48, 2004, pp. 18601–18607.

[14] Chang, I. T. H., and Ren, Z., "Simple Processing Method and Characterisation of Nanosized Metal Powders," *Materials Science and Engineering A*, Vols. 375–377, July 2004, pp. 66–71.

[15] Mang, J. T., Hjelm, R. P., Peterson, P. D., Jorgensen, B. S., and Son, S. F., "Characterization of Components of Nano-Energetics by Small-Angle Scattering Techniques," *Proceedings of the 31st International Pyrotechnics Seminar*, edited by F. J. Schelling, IPSUSA Seminars, Inc., Marshall, TX, 2004, pp. 299–305.

[16] Son, S. F., "Performance and Characterization of Nanoenergetic Materials at Los Alamos," in *Synthesis, Characterization and Properties of Energetic/Reactive Nanomaterials: Materials Research Society Symposium Proceedings*, edited by R. Armstrong, N. Thadhani, W. Wilson, J. Gilman, and R. Simpson, Vol. 800, Materials Research Society, Warrendale, PA, 2004, pp. 161–172.

[17] Bockmon, B. S., Pantoya, M. L., Son, S. F., Asay, B. W., and Mang, J. T., "Combustion Velocities and Propagation Mechanisms of Metastable Interstitial Composites," *Journal of Applied Physics*, Vol. 98, No. 6, 2005, pp. 064903-1–064903-7.

[18] Pantoya, M. L., Son, S. F., Danen, W., Jorgensen, B., Asay, B. W., Busse, J., and Mang, J., "Characterization of Metastable Intermolecular Composites (MIC's)," in *Defense Applications of Nanomaterials*, ACS Symposium Series 891, edited by A. W. Miziolek, S. P. Karna, J. M. Mauro, and R. A. Vaia, American Chemical Society Publications, Washington, D.C., 2005, pp. 227–240, Chap. 16.

[19] Park, K., Lee, D., Rai, A., Mukherjee, D., and Zachariah, M. R., "Size-Resolved Kinetic Measurements of Aluminum Nanoparticle Oxidation with Single Particle Mass Spectrometry," *Journal of Physical Chemistry B*, Vol. 109, No. 15, 2005, pp. 7290–7299.

[20] Jouet, R. J., Warren, A. D., Rosenberg, D. M., Bellitto, V. J., Park, K., and Zachariah, M. R., "Surface Passivation of Bare Aluminum Nanoparticles Using Perfluoroalkyl Carboxylic Acids," *Chemistry of Materials*, Vol. 17, No. 11, 2005, pp. 2987–2996.

[21] Johnson, C. E., and Higa, K. T., "Preparation of Nanometer Sized Aluminum Powder," *Nanophase and Nanocomposites Materials II: Materials Research Society Symposium Proceedings*, edited by S. Komarneni, J. C. Parker, and H. J. Wollenberger, Vol. 457, Materials Research Society, Warrendale, PA, 1997, pp. 131–135.

[22] Tompa, A. S., Boswell, R. F., Skahan, P., and Gotzmer, C., "Low/High Temperature Relationships in Dinitramide Salts by DEA/DSC and Study of Oxidation of Aluminum Powders by DSC/TG," *Journal of Thermal Analysis*, Vol. 49, No. 3, 1997, pp. 1161–1170.

[23] Mench, M. M., Kuo, K. K., Yeh, C. L., and Lu, Y. C., "Comparison of Thermal Behavior of Regular and Ultra-Fine Aluminum Powders (Alex) Made from Plasma Explosion Process," *Combustion Science and Technology*, Vol. 135, No. 1–6, 1998, pp. 269–292.

[24] Ivanov, V. G., and Gavrilyuk, O. V., "Specific Features of the Oxidation and Self-Ignition of Electroexplosive Ultradisperse Metal Powders in Air," *Combustion, Explosion and Shock Waves*, Vol. 35, No. 6, 1999, pp. 648–655.

[25] Jones, D. E. G., Brousseau, P., Fouchard, R. C., Turcotte, A.-M., and Kwok, Q. S. M., "Thermal Characterization of Passivated Nanometer Size Aluminium Powders," *Journal of Thermal Analysis and Calorimetry*, Vol. 61, No. 3, 2000, pp. 805–818.

[26] Pivkina, A., Streletskii, A., Kolvanev, I., Ul'yanova, P., Frolov, Yu., Butyagin, P., and Schoonman, J., "Mechanochemically Activated Nano-Aluminium: Oxidation Behavior," *Journal of Materials Science*, Vol. 39, No. 16–17, 2004, pp. 5451–5453.

[27] Puszynski, J. A., "Reactivity of Nanosize Aluminum with Metal Oxides and Water Vapor," in *Synthesis, Characterization and Properties of Energetic/Reactive Nanomaterials: Materials Research Society Symposium Proceedings*, edited by R. Armstrong, N. Thadhani, W. Wilson, J. Gilman, and R. Simpson, Vol. 800, Materials Research Society, Warrendale, PA, 2004, pp. 223–232.

[28] Smith, B. L., Jorgensen, B. S., Busse, J. R., Ferris, M. J., and Danen, W. C., "Determination of Oxide Layer Thickness of Aluminum Nanoparticles," Los Alamos National Laboratory, LA-UR-01-1665, Los Alamos, NM, 2001.

[29] Walter, K. C., Aumann, C. E., Carpenter, R. D., O'Neill, E. H., and Pesiri, D. R., "Energetic Materials Development at Technanogy Materials Development," in *Synthesis, Characterization and Properties of Energetic/Reactive Nanomaterials: Materials Research Society Symposium Proceedings*, edited by R. Armstrong, N. Thadhani, W. Wilson, J. Gilman, and R. Simpson, Vol. 800, Materials Research Society, Warrendale, PA, 2004, pp. 27–38.

[30] Eisenreich, N., Fietzek, H., Juez-Lorenzo, M. d. M., Kolarik, V., Koleczko, A., and Weiser, V., "On the Mechanism of Low Temperature Oxidation for Aluminum Particles down to the Nano-Scale," *Propellants, Explosives, Pyrotechnics*, Vol. 29, No. 3, 2004, pp. 137–145.

[31] Johnson, C. E., Higa, K. T., and Chafin, A., "Nano Aluminum Size Distribution from TGA Analysis," *Proceedings of the 32nd JANNAF Propellant & Explosives Development and Characterization Subcommittee Meeting*, Chemical Propulsion Information Agency Publication JSC CD-34, Chemical Propulsion Information Agency, Columbia, MD, 2004.

[32] Higa, K. T., Johnson, C. E., and Hollins, R. A., "Preparation of Fine Aluminum Powders by Solution Methods," U.S. Patent 5 885 321, 23 March 1999.

[33] Foley, T., Johnson, C., and Higa, K., "Inhibition of Oxide Formation on Aluminum Nanoparticles by Transition Metal Coating," *Chemistry of Materials*, Vol. 17, No. 16, 2005, pp. 4086–4091.

[34] Kramer, G. W., Levy, A. B., and Midland, M. M., "Laboratory Operations with Air-Sensitive Substances: Survey," in H. C. Brown, *Organic Synthesis via Boranes*, Wiley, New York, 1975, pp. 241–245.

[35] Klug, H. P., and Alexander, L. E., *X-Ray Diffraction Procedures for Polycrystalline and Amorphous Materials*, 2nd ed., Wiley, New York, 1974, p. 687.

[36] Gregg, S. J., and Sing, K. S., *Adsorption, Surface Area and Porosity*, 2nd ed., Academic Press, New York, 1982.

[37] Brunauer, S., Emmett, P. H., and Teller, E., "Adsorption of Gases in Multimolecular Layers," *Journal of the American Chemical Society*, Vol. 60, No. 2, 1938, pp. 309–319.

[38] Trunov, M. A., Schoenitz, M., and Dreizin, E. L., "Ignition of Aluminum Powders Under Different Experimental Conditions," *Propellants, Explosives, Pyrotechnics*, Vol. 30, No. 1, 2005, pp. 36–43.

[39] Suvaci, E., Simkovich, G., and Messing, G. L., "The Reaction-Bonded Aluminum Oxide Process, 1: The Effect of Attrition Milling on the Solid-State Oxidation of Aluminum Powder," *Journal of the American Ceramic Society*, Vol. 83, No. 2, 2000, pp. 299–305.

[40] Kwok, Q. S. M., Fouchard, R. C., Turcotte, A.-M., Lightfoot, P. D., Bowes, R., and Jones, D. E. G., "Characterization of Aluminum Nanopowder Compositions," *Propellants, Explosives, Pyrotechnics*, Vol. 27, No. 4, 2002, pp. 229–240.

[41] Risha, G. A., Boyer, E., Wehrman, R. B., and Kuo, K. K., "Performance Comparison of HTPB-Based Solid Fuels Containing Nano-Sized Energetic Powder in a Cylindrical Hybrid Rocket Motor," AIAA Paper 2002-3576, 2002.

[42] Jones, D. E. G., Turcotte, R., Fouchard, R. C., Kwok, Q. S. M., Turcotte, A.-M., and Abdel-Qader, Z., "Hazard Characterization of Aluminum Nanopowder Compositions," *Propellants, Explosives, Pyrotechnics*, Vol. 28, No. 3, 2003, pp. 120–131.

[43] Trunov, M. A., Schoenitz, M., Zhu, X., and Dreizin, E. L., "Effect of Polymorphic Phase Transformations in Al_2O_3 Film on Oxidation Kinetics of Aluminum Powders," *Combustion and Flame*, Vol. 140, No. 4, 2005, pp. 310–318.

[44] Shevchenko, V. G., Kononenko, V. I., Latosh, I. N., Chupova, I. A., and Lukin, N. V., "Effect of the Size Factor and Alloying on Oxidation of Aluminum Powders," *Combustion, Explosion and Shock Waves*, Vol. 30, No. 5, 1994, pp. 635–637.

[45] Il'in, A. P., Yablunovskii, G. V., Gromov, A. A., Popenko, E. M., and Bychin, N. V., "Combustion of Mixtures of Ultrafine Powders of Aluminum and Boron in Air," *Combustion, Explosion and Shock Waves*, Vol. 35, No. 6, 1999, pp. 656–659.

[46] J. E. Hatch (ed.), *Aluminum: Properties and Physical Metallurgy*, American Society for Metals, Metals Park, OH, 1984, p. 17.

[47] Phung, X., Groza, J., Stach, E. A., Williams, L. N., Ritchey, S. B., "Surface Characterization of Metal Nanoparticles," *Materials Science and Engineering A*, Vol. 359, No. 1–2, 2003, pp. 261–268.

[48] Kwon, Y.-S., Gromov, A. A., Ilyin, A. P., and Rim, G.-H., "Passivation Process for Superfine Aluminum Powders Obtained by Electrical Explosion of Wires," *Applied Surface Science*, Vol. 211, No. 1–4, 2003, pp. 57–67.

[49] Ramaswamy, A. L., and Kaste, P., "A 'Nanovision' of the Physiochemical Phenomena Occurring in Nanoparticles of Aluminum," *Journal of Energetic Materials*, Vol. 23, No. 1, 2005, pp. 1–25.

[50] Johnson, C., Parr, T., Hanson-Parr, D., Hollins, R., Fallis, S., and Higa, K., "Combustion and Oxidation of Metal Nanoparticles and Composite Particles," *Proceedings of the 37th JANNAF Combustion Subcommittee Meeting*, Chemical Propulsion Information Agency Publication 701, Vol. 1, Chemical Propulsion Information Agency, Columbia, MD, 2000, pp. 539–551.

[51] Hunter, M. S., and Fowle, P., "Natural and Thermally Formed Oxide Films on Aluminum," *Journal of the Electrochemical Society*, Vol. 103, No. 9, 1956, pp. 482–485.

[52] Smeltzer, W. W., "Oxidation of Aluminum in the Temperature Range

400–600°C," *Journal of the Electrochemical Society*, Vol. 103, No. 3, 1956, pp. 209–214.

[53] Blackburn, P. E., and Gulbransen, E. A., "Aluminum Reactions with Water Vapor, Dry Oxygen, Moist Oxygen, and Moist Hydrogen Between 500° and 625°C," *Journal of the Electrochemical Society*, Vol. 107, No. 12, 1960, pp. 944–950.

[54] Zhu, X., Schoenitz, M., and Dreizin, E. L., "Oxidation Processes and Phase Changes in Metastable Al–Ti Mechanical Alloys," in *Synthesis, Characterization and Properties of Energetic/Reactive Nanomaterials: Materials Research Society Symposium Proceedings*, edited by R. Armstrong, N. Thadhani, W. Wilson, J. Gilman, and R. Simpson, Vol. 800, Materials Research Society, Warrendale, PA, 2004.

S. Son
Associate Editor